ULTRACOLD HYDROGEN

Principal Investigators:
Professor Daniel Kleppner and Professor Thomas J. Greytak

Project Staff:
Professor Theodore Ducas (Wellesley College), Joel DeVries, Walter Joffrain, Cort Johnson, Philippe Larochelle, Sourav Mandal, Stephen C. Moss, David Landhuis, Dr. Lorenz Willmann, Lia Matos, Margaret Pan, Thomas Schibli, Julia K. Steinberger, Kendra Vant

Sponsors:
National Science Foundation, Office of Naval Research, Center for Ultracold Atoms at MIT and Harvard

Research in Ultracold Hydrogen
Research in the Ultracold Hydrogen Group centers on studies of atomic hydrogen as a quantum gas, the atomic physics of hydrogen, and ultra high precision spectroscopy. Principal activities during the past year were a theoretical and experimental study of the growth dynamics of a Bose-Einstein condensate in hydrogen, and a study of collisions between metastable hydrogen atoms. The work is being prepared for publication. Moving in a new direction, work has been started on ultrahigh resolutions spectroscopy of hydrogen. The initial goal will be to advance the precision on two-photon 2S -(8-12)S transitions. In a separate experiment carried out by members of the group, a new value for the Rydberg constant was measured by millimeter wave spectroscopy on Rydberg states of hydrogen. The results are consistent with current values obtained by optical spectroscopy, and are being prepared for publication.

Reports on Research

THE PHYSICS OF HYDROGEN 2S - 2S COLLISIONS

Introduction
Detecting atomic hydrogen optically is experimentally challenging because its principal transition, L-α (121 nm) lies in a UV region where lasers are not practical and the optics offers special problems. Consequently, in our studies of ultracold hydrogen and Bose-Einstein condensation in atomic hydrogen we have used laser excitation of the two-photon 1S -2S transition (243 nm) as the principal diagnostic tool. In these experiments the density of trapped hydrogen can be greater than 10^{14} cm^{-3}, and the laser excitation rate can be greater than 10^{8} atoms/s. The natural lifetime of the 2S state is 0.12 s, and in consequence the density of 2S atoms can become significant. The cloud of 2S atoms can provide an unprecedented source for precise optical spectroscopy of hydrogen. In addition, it is also of intrinsic interest because of the unusual nature of the 2S state: the simplest excited state of an atom.

At high densities, 2S - 2S collisions can limit the 2S population through inelastic processes. Those processes could never be directly observed in the past because of the lack of 2S atoms. We describe here the results of the first study of 2S - 2S collisions.

Experimental approach
After preparing a cold, dense sample of ground state H in our magnetic trap, it is possible to excite clouds of more than 10^{7} metastable H atoms with a 2 ms pulse of UV laser. This cloud quickly thermalizes with the surrounding ground state sample, and it can last for times comparable to the 122 ms natural lifetime of the 2S state. Since the magnetic moment of the 2S atoms produced is almost identical to that of the trapped 1S atoms, the metastable clouds produced by 1S - 2S excitation are also trapped. By generating trapped metastable H in this

way, we have been able to perform the first measurements of 2S - 2S inelastic rate constants at low temperatures. [1,2]

Our metastable hydrogen clouds are also interesting spectroscopic samples in their own right. Much work has already been completed in the MIT Ultracold Hydrogen group towards developing diode laser systems to probe transitions originating in the 2S state. The two-photon transitions to higher-lying S states are of particular interest. Taking advantage of advances in optical frequency metrology [3], our group plans to measure the absolute frequency of one or more of these 2S - nS transitions with unprecedented accuracy. In combination with the recent exquisitely precise determination of the 1S - 2S transition frequency [4], these measurements will not only test the state-of-the-art of quantum electrodynamics (QED) theory for the hydrogen atom [5,6] but will also provide a new value for the Rydberg constant [6], which relates several fundamental constants.

Inelastic Collisions

Metastable H atoms excited from a gas of trapped ground state atoms can participate in several types of inelastic collisions. The physics of these interactions is potentially very rich. Stimulated by our experimental investigations, a body of theoretical work on metastable H collisions [7,8,9] is developing. In particular, R. Forrey and collaborators have made the first calculations of 2S - 2S collisional rate constants extending to T = 0 [8].

The inelastic collisions of metastable hydrogen in a background gas of ground state hydrogen fall into three categories: excitation transfer collisions, ionizing collisions, and hyperfine-changing collisions. In an excitation transfer collision, at least one 2S atom undergoes a transition to the 2P state and subsequently decays by emission of a Lyman-α photon. Ionizing collisions come in at least two flavors: associative ionization, in which two 2S atoms collide and form an H_2^+ molecule, and Penning ionization, in which the internal energy of one 2S atom causes the ionization of another 2S atom. Hyperfine-changing collisions, mediated by weak magnetic dipole interactions, are predicted to have rate constants which are orders of magnitude smaller than the other inelastic processes. Nevertheless, 1S - 2S hyperfine-changing collisions may occur frequently in our samples due to the large 1S density.

From measurements of metastable number decay, it is possible to distinguish between loss rates due to 2S - 2S and 1S - 2S inelastic collisions. The former are two-body processes, which the latter, like collisions with a background gas, are one-body metastable loss processes. (Three-body loss is not expected to be significant at the densities in our experiments.) By fitting decay data to a model incorporating both one- and two-body loss terms, we can determine total rate constants for loss due to inelastic collisions.

Decay Measurements

The decay of the metastable cloud has been studied systematically in four different trap configurations, each with a different sample temperature and peak ground state density. We label these samples W, X, Y, and Z, and their location in phase space is depicted in Figure 1.

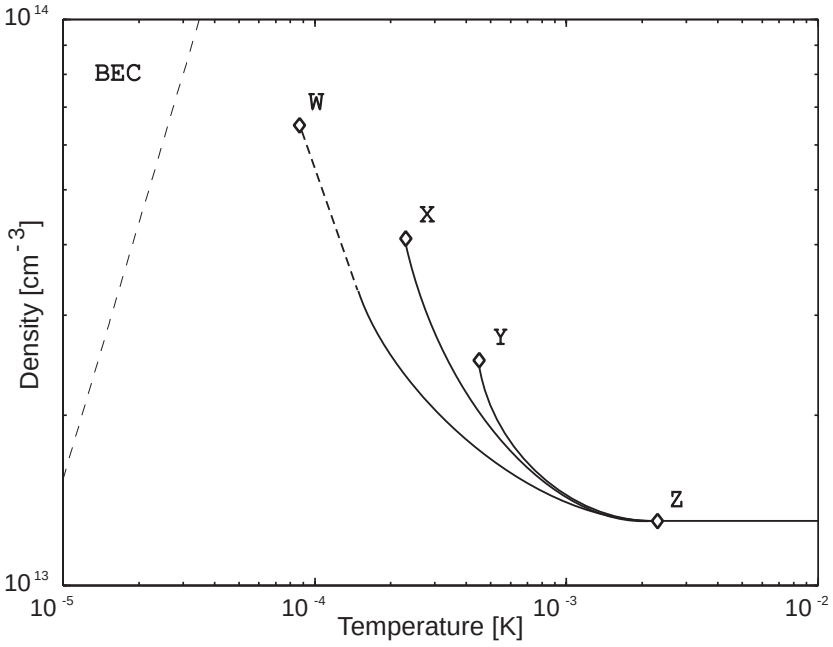

Figure 1; Temperature and peak density of ground state H samples in which decay studies of metastable clouds were performed. The solid lines roughly indicate the trajectory of the samples during magnetic saddlepoint evaporation, originating from higher temperatures at right. A dashed line denotes the approximate rf evaporation trajectory of trap W. A longer dashed line marks the boundary between the BEC and normal phase of the gas.

By varying the wait time between the excitation pulse and the quenching detection pulse, we mapped the decay behavior of the metastable cloud. The number of Lyman-α photons detected at each quench pulse is proportional to the number of metastable atoms remaining in the trap. In a typical measurement of a single decay curve, eight different wait times were used, and an excitation pulse occurred every 100 ms. Thus, a decay curve was recorded every 800 ms, and approximately 100 decay measurements were made before the ground state sample was depleted. The laser frequency was swept back and forth across the 1S - 2S resonance, and a wide range of different initial metastable numbers were excited in each trap.

In the colder, denser samples (W and X), where the largest metastable populations were generated, the decay behavior was found to be qualitatively different depending on how many metastables were excited (see Figures 2). A simple model which can be used to fit the decay curves at both high and low metastable numbers is the “one-plus-two" model:

$$s(t) = \alpha_1 A_o \, e^{-[\alpha_1 t]} / [\alpha_1 + \alpha_2 A_o \, (1 - e^{-[\alpha_1 t]})], \qquad (1)$$

where s(t) is the metastable signal as a function of time after excitation, and $A_o = s(0)$. If the relative spatial distribution of metastables is approximately static as the cloud decays, then α_1 and α_2 are simply related to the rate constants for one-body and two-body loss. Equation 1 is the solution to the differential equation

$$ds/dt = -\alpha_1 s - \alpha_2 s^2 \qquad (2)$$

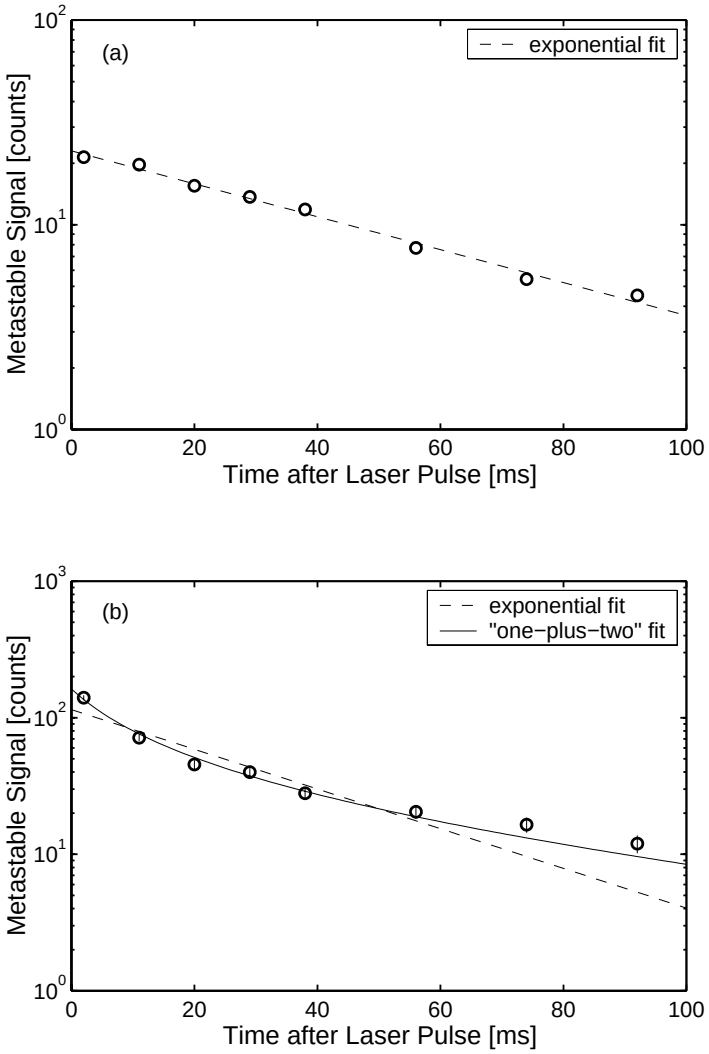

Figure 2: Semi-logarithmic plots of decay data at two different signal levels in trap W. In plot (a), which is the average 60 decay curves with approximately the same initial metastable signal, a simple exponential describes the decay well. For (b), which is the average of two decay curves with an initial signal more than 6 times as large, the data is better described by a "one-plus-two" model which includes terms corresponding to both one- and two-body loss.

In the limit of small metastable signal, the one-plus-two model reduces to a simple exponential decay. When fitting the decay data, α_1 was first determined by extrapolating the decay behavior to the limit of zero metastable number. Individual decay curves could then be fit using only two free parameters: α_2 and A_o.

Determination of Rate Constants

It can be shown that, in the approximation of a static 2S cloud shape, the total two-body loss rate constant K_2 is related to observations by

$$K_2 = \zeta \varepsilon \alpha_2 \qquad (3)$$

where ζ is a geometry factor, dependent on the shape of the metastable cloud, and ε is the detection efficiency for metastables. The geometry factor ζ can be calculated numerically based on the known magnetic trap shape and the location and size of the laser focus. The detection efficiency can be calibrated to within 30-60% by depleting a ground state sample by 1S - 2S

excitation and recording the total number of signal counts. To account for the fact that the metastable distribution along the trap axis tends to flatten because of density-dependent loss and diffusion of the 2S atoms in the background 1S sample, a dynamic simulation of the metastable cloud was developed. The simulation yielded a correction factor to multiply the expression in Eq. 3.

The experimental results for K_2 in the four different traps are compared with the current theory in Fig. 3. For traps Y and Z, the experimental results for K_2 were consistent with zero, total systematic uncertainty was used to establish upper bounds. The theoretical curve is given by

$$K_2 = 2\,(R_{et} + R_{ion})\,, \qquad (4)$$

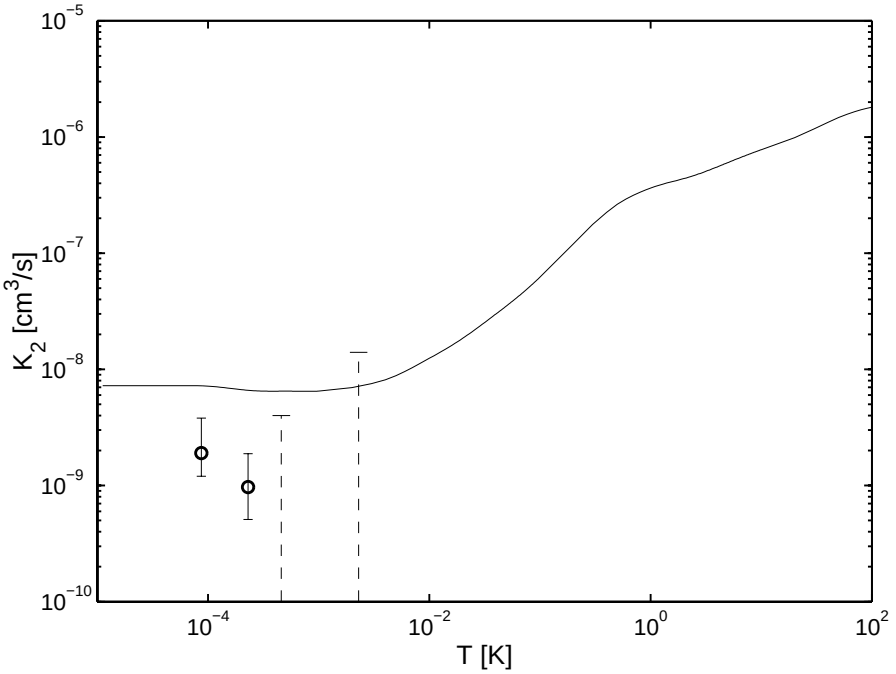

Figure 3: Theoretical and experimental values for K_2 as a function of temperature. The solid curve is the sum of theoretical loss rate constants for 2S - 2S excitation transfer and ionization processes, calculated by R. Forrey and collaborators. Experimental values are indicated by circles. At the temperatures where only upper limits were determined, dashed lines indicate the range of possible values for K_2.

where R_{et} and R_{ion} are the theoretical rate constants for double excitation transfer and ionization, respectively. All other two-body loss processes are assumed to be negligible relative to these. Since the current theory does not yet include hyperfine interactions or the effects of the magnetic trapping fields, the theoretical curve is considered to be an order-of-magnitude calculation. Theory and experiment are thus well in range of one another.

From the variation of α_1 with ground state density in each trap, it is possible to set an experimental upper bound on the 1S - 2S loss rate constant for metastables, K_{12}. The upper limit was found to be a few times 10^{-13} cm^3/s in traps W, X, and Y, and about 10^{-12} cm^3/s in trap Z. It is possible that K_{12} is much larger than the total 1S - 1S inelastic constant, $g_{eff} \approx 1 \times 10^{-15}$ cm^3/s. If this turns out to be the case, it would suggest that 1S - 2S excitation transfer collisions are much more probable than hyperfine-changing collisions.

THE GROWTH AND DECAY OF A BOSE-EINSTEIN CONDENSATE IN HYDROGEN

Introduction

In the period immediately preceding the 1995 observation of Bose-Einstein condensation (BEC) in trapped atomic gases, theorists debated the likely rate of condensate formation. The experimental observation of condensates in Rb [10], Na [11], and Li [12] proved that condensates form in a relatively short time, and the excitement surrounding the discovery of BEC shifted most activity into the investigation of the equilibrium properties of these novel systems.

Hydrogen condensates share many characteristics with condensates of alkali metal atoms, but there are several notable differences. Among these is the anomalously small s-wave scattering length, a. Consequences of the small scattering length include large condensate densities and a low elastic scattering rate. The low scattering rate retards evaporative cooling and complicates the production of H condensates, but it also increases the time scale for formation of the condensate, simplifying the task of studying condensate growth in detail.

In the past year we have performed detailed experimental and theoretical studies of the formation and decay of a Bose-Einstein condensate of atomic hydrogen. In this report, we will briefly describe the experimental techniques used to observe the formation of a hydrogen condensate. We will then examine a sample of the experimental data. In the final section of this report, we will make a quantitative comparison between theory and experiment.

Experiment:

RF Evaporation

A central technique for carrying out condensate growth experiments is radio frequency (rf) evaporation. To reach temperatures below 200 μK we apply an rf field that causes transitions to an untrapped magnetic sublevel wherever the trapping magnetic field satisfies the resonance condition. To perform forced evaporation and cool the trapped sample, we slowly reduce the frequency of the rf field. This has the effect of removing only the most energetic atoms from the trap while allowing the remaining atoms to redistribute energy. In this way the temperature of the sample is reduced. During rf evaporation the rf frequency is reduced slowly so that the trapped atomic sample remains in thermal equilibrium.

RF Cut Experiment

In order to make quantitative comparisons with theory, manipulated the trapped sample with rf magnetic fields. We stimulated the formation of a condensate by rapidly changing the applied rf frequency. RF evaporation was used to cool the thermal cloud to a temperature just above the transition temperature. The final frequency of the rf evaporation sweep, ε_{start}, controls the temperature of the sample, allowing the thermal cloud to be prepared in a well-defined initial state. A nonequilibrium situation was then created by rapidly lowering the rf frequency from ε_{start} to a final value, ε_{rf}, and holding it fixed. This rapid rf sweep, or “cut", had the effect of truncating the high-energy tail of the energy distribution, leaving the sample unstable against condensate formation. We monitored the 1S-2S spectrum from the end of rf evaporation through the rf cut and hold. In this way, we recorded the formation and decay of a single Bose-Einstein condensate. This differs from many alkali atom experiments in which the detection process destroys the condensate and the experiment must be repeated many times for nominally identical initial conditions [13, 14].

We performed rf cut experiments in which the ending rf frequency, ε_{rf}, was kept constant while the starting rf frequency, ε_{start}, was varied. This procedure allowed us to prepare the noncondensed sample at various points in phase space away from the Bose-Einstein transition and then truncate the thermal distribution with an rf cut, making the system unstable against condensate formation.

The scheme for varying the trap depth is shown in Fig. 4. Three separate rf cuts were performed. The ending frequency of rf evaporation took values of 8.1, 7.7, and 7.3 Mhz. An rf cut of t_rf = 1 s was carried out with an ending frequency of ε_{rf} = 4.5 MHz. These cuts resulted in initial trap depths of 5.35(2) MHz (257 μK), 4.95(2) MHz (238 μK), and 4.55(2) MHz (218 μK); and a final trap depth of 1.75(2) MHz (84 μK).

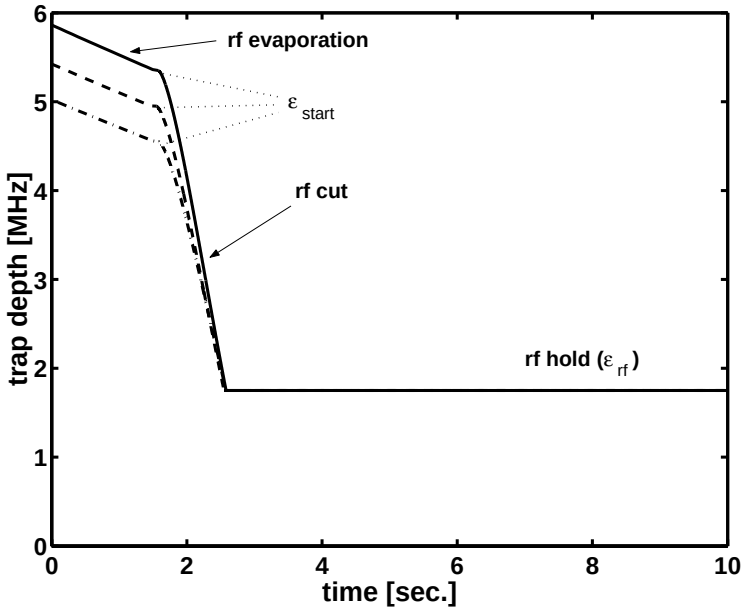

Figure 4: Trap depth versus time for experiments in which ε_{rf} is held constant and ε_{start}t is varied. By changing the frequency at which the rf cut begins, the noncondensed sample is prepared at various distances in phase space from the Bose-Einstein transition. After the rf cut the trap depth is held constant, and the condensate formation is monitored spectroscopically.

During the rf cut experiment the condensate signal was monitored by rapidly sweeping the laser frequency across the Doppler-sensitive 1S - 2S spectrum. The recorded spectrum has two major components: a relatively narrow, strong signal due to condensed atoms and a broad, weak signal (the Doppler profile) due to noncondensed atoms. The cold-collision frequency shift causes the condensate signal to appear to the red of the center of the Doppler profile. By recording the signal to the blue of the center, the Doppler profile can be subtracted from the total signal, leaving only the condensate signal.

Figure 5 presents the total condensate signal versus time after the counts due to the Doppler profile and background fluorescence have been removed. The end of the t_{rf} = 1 s rf cut is delineated by the vertical dashed line in each panel, and the final trap depth is the same in each case: 1.75(2) MHz. The salient feature of these traces is the relative delay between the end of the rf cut and the onset of condensate formation. The open circles (o) represent the sample that was prepared closest to the Bose-Einstein transition prior to the cut. Following the cut the sample cooled for less than a second before a condensate began to form. In contrast the sample represented by the open triangles (∆) underwent significant cooling following the rf cut prior to the appearance of a condensate. The delay is understandable since this sample was prepared further from the transition in a deeper trap.

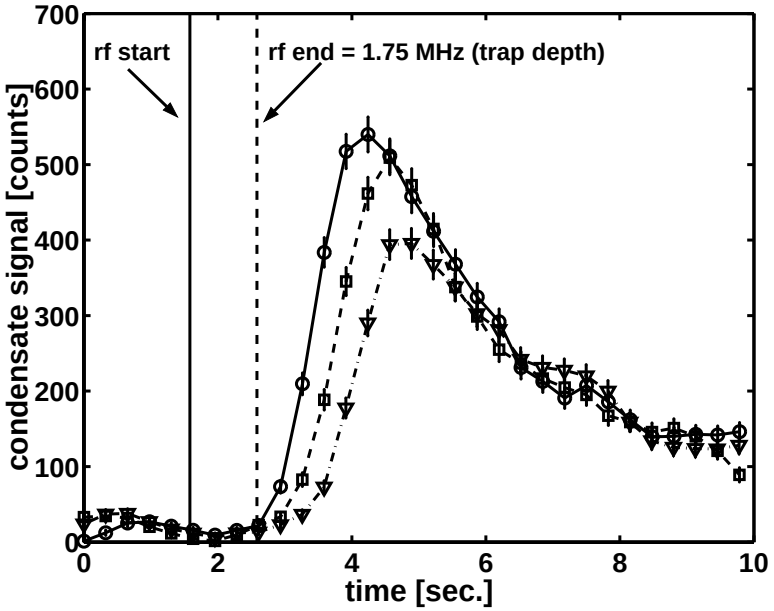

Figure 5: Time evolution of the condensate signal for experiments in which ε_{rf} is held constant and ε_{start} is varied. For each time point the condensate signal is summed over frequency and the Doppler profile subtracted. The resulting signal is passed through a smoothing filter and plotted versus time. The open circles (o) represent the sample with 4.55(2) MHz initial trap depth, the open boxes 4.95(2) MHz, and the open triangles 5.35(2) MHz. The sample prepared closest to degeneracy (o) results in the largest and earliest condensate. The sample prepared furthest from the Bose-Einstein transition (∆) cools significantly following the rf cut and results in a smaller, delayed condensate. An intermediate case is given by the open boxes. Interestingly, after about 6 s the signals are indistinguishable, indicating that a dynamic equilibrium has been reached between the normal gas and condensate at this particular trap depth, 1.75(2) MHz. The lines connecting the data points serve as guides to the eye.

The physics underlying this experiment is relatively simple to understand. For a condensate to form, a significant number of atoms need to be present in the lowest energy eigenstates of the trap. For the same magnetic trap and sample preparation procedure, a deeper trap will contain a warmer sample, and the warmer sample will contain fewer atoms in low energy states. Swift removal of atoms in the highest energy states, i.e. an rf cut, initiates a change in the energy distribution of the sample as it attempts to find an equilibrium temperature in the suddenly shallower trap. The larger the change in trap depth, the longer the time required for the sample to find its new equilibrium.

Figure 5 makes the different condensate sizes apparent in the amplitudes of the three signals. Intuitively it is sensible that the sample prepared closest to the transition results in the earliest and largest condensate. After t = 6 s, however, the three signals become indistinguishable. The history of how early the condensate formed or how large it became seems to be unimportant. Most likely the system finds a new equilibrium for a particular condensate size and trap depth. Once this equilibrium is found, the system can evolve in only one way.

Comparison with Theory

In atomic hydrogen decay of the trapped gas due to inelastic two-body collisions has a significant influence on the formation of the condensate and must be included for quantitative comparison of theory with experiment. Previous theoretical work was devoted primarily to understanding the ^{23}Na experiment [15] and did not require a description of the decay of the gas [16, 17, 18]. In

collaboration with Professor Henk Stoof [1] we have extended the work of Bijlsma et al. [16] to include decay processes and the effects of rf evaporation on the thermal cloud.

Figure 6 shows the condensate growth data and the results of simulations for experiments in which the starting point of the rf cut, ε_{start}, was varied. The agreement is good, and the trends in the initial atom number, N_{start}, initial temperature, T_{start}, are reasonable. Recall that in these experiments the noncondensed sample was cooled to just above the Bose-Einstein transition temperature before a t_{rf} = 1 s_{rf} cut lowered the trap depth to just 84 μK. The end of the rf cut is shown in each panel. The upper panel shows the time evolution of the condensate number for the sample that started furthest from the transition with an initial trap depth of 257 μK. As expected this sample had the largest initial number of atoms, N_{start} = 2.92 times 10^{10}, and the highest temperature, T_{start} = 36 μK. In the other two panels, the rf cut begins with the sample closer to the transition. The trap depths are shallower, and the corresponding initial atom number and temperature are lower. The middle panel shows the growth of the condensate with N_{start} = 2.81 X 10^{10} and T_{start} = 35 μK with an initial trap depth of 238 μK. In the lower panel, N_{start} = 2.81 X 10^{10} and T_{start} = 35 μK for an initial trap depth of 218 μK.

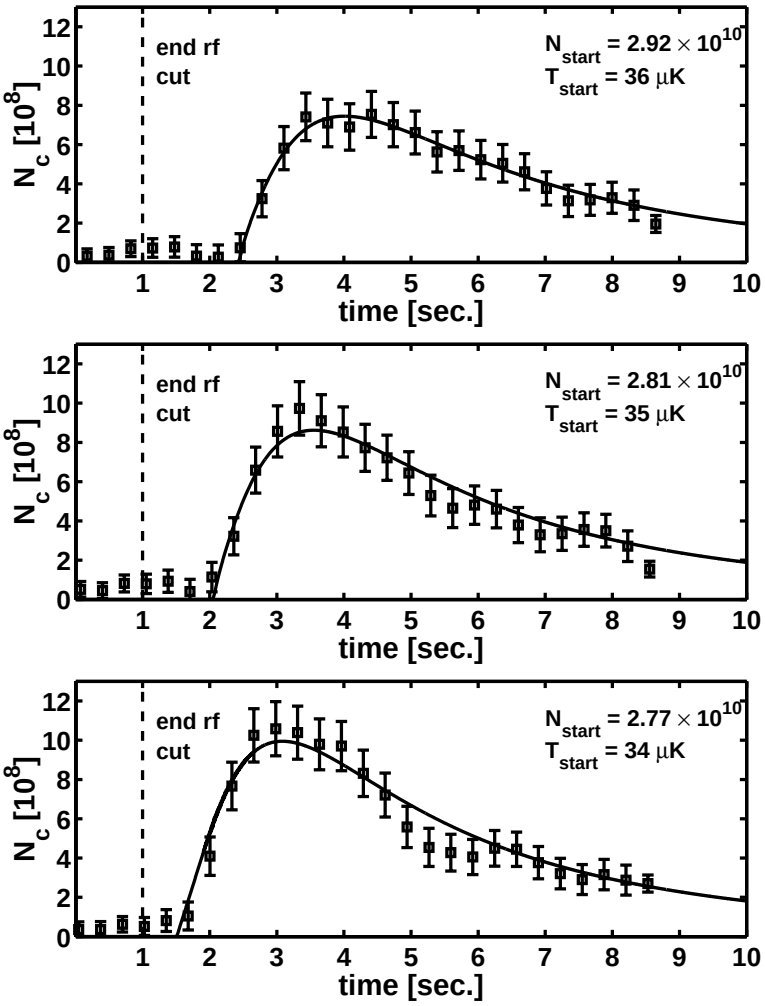

Figure 6: Comparison of calculations with experiments in which $\varepsilon_{start}t$ was varied. The initial atom number and temperature are indicated in each panel.

[11] Institute for Theoretical Physics, University of Utrecht, The Netherlands

The sensible values of N_{start}, T_{start} required to obtain good agreement between calculation and the experiments presented above give us confidence that we have determined the condensate population as a function of time. More broadly, we have gained insight into the dynamics of a system near a second-order phase transition

Articles

Thomas J. Greytak and Daniel Kleppner, “Bose-Einstein condensation", in *McGraw-Hill Yearbook of Science and Technology 2001*, p. 64.

Ultracold Hydrogen, Lorenz Willmann and Daniel Kleppner, *The Hydrogen Atoms,* S.G. Kareshenboim, F.S. Pavone, F. Bassani, M. Inguscio, T.W. Haensch, Eds., (Springer 2001), p. 42.
Splitting the Second: The story of atomic time (book review), Nature **410**, 1027, (2001).

Beyond Quantum Mechanics: Insights from the work of Martin Gutzwiller, Daniel Kleppner and John B. Delos, Foundations of Physics, **31**, 593 (2001).

Classically-Forbidden Process in Photoabsorption Spectra, V. Kondratovich, J.B. Delos, D. Kleppner and N. Spellmeyer, Phys. Rev. A **64,** 3409, 2000.

Theses

DeVries, Joel C, *A Precision Millimeter Wave Measurement of the Rydberg Frequency,* Ph.D. Thesis, MIT 2001.

Pan, Margaret, *Work on Diode Lasers for Spectroscopy of Atomic Hydrogen,* Senior Thesis, Department of Physics, MIT 2001.

References

[1] D. Landhuis, Ph.D. thesis, Harvard University, 2002.

[2] D. Landhuis, L. Matos, S.C. Moss, K. Vant, J.K. Steinberger, L. Willmann, T.J. Greytak, and D. Kleppner, in preparation.

[3] T. Udem, J. Reichert, R. Holzwarth, and T.W. Haench, Optics Letters, **24**, 881 (1999).

[4] M. Niering, R. Holzwarth, J. Reichert, P. Pokasov, T. Udem, M. Weitz and T.W. Haensch, Phys. Rev. Lett. **84**, 5496 (2000).

[5] K. Pachucki, Phys. Rev. A **63**, 042503 (2001).

[6] C. Schwob, L. Jozefowski, B. deBeauvoir, L. Hilico, F. Nez, L. Julien, and F. Biraben, Phys. Rev. Lett. **82**, 4960 (1999).

[7] R.C. Forrey, R. Cote, A. Dalgarno, S. Jonsell, A. Saenz, and P. Froelich, Phys. Rev. Lett. **85**, 4245 (2000).

[8] R.C. Forrey, S. Jonsell, P. Froelich, A. Saenz and A. Dalgarno, to be published.

[9] S. Jonsell, A. Saenz, P. Froelich, R. C. Forrey, R. Cote and A. Dalgarno, to be published.

[10] M.H. Anderson, J.R. Ensher, M.R. Matthews, C.E. Wieman, and E.A. Cornell, Science **269**, 198 (1995).

[11] K.B. Davis, M.-O. Mewes, M.R. Andrews, N.J. van Druten, D.S. Durfee, and W. Ketterle, Phys. Rev. Lett. **75**, 3969 (1995).

[12] C.C. Bradley, C.A. Sackett, J.J. Tollett, and R.G. Hulet, Phys. Rev. Lett. **75**, 1687 (1995).

[13] J.M. Gerton, D. Strekalov, I. Prodan, and R.G. Hulet, Nature, **408**, 692 (2000).

[14] M. Kohl, T.W. Haensch, and T. Esslinger, cond-mat/0106642 (2001).

[15] H.-J. Miesner, D.M. Stamper-Kurn, M.R. Andrews, D.S. Durfee, S. Inouye, and W. Ketterle, Science **279**, 1005 (1998).

[16] M.J. Bijlsma, E. Zaremba, and H.T.C. Stoof, Phys. Rev. A **62**, 063609 (2000).

[17] M.J. Davis, C.W. Gardiner, and R. J. Ballagh, Phys. Rev. A **62**, 063608 (2000).

[18] C.W. Gardiner, P. Zoller, R.J. Ballagh, and M.J. Davis, Phys. Rev. Lett. **79**, 1793 (1997).